

Low cycle fatigue of pseudoelastic NiTi alloys

C. Maletta¹, E. Sgambitterra¹, F. Furgiuele¹, R. Casati² and A. Tuissi²

¹ Department of Mechanical Engineering, University of Calabria, P. Bucci 46 C, 87036 Rende (Italy), Fax: +39 0984494673, carmine.maletta@unical.it

² National Research Council -Institute for Energetics and Interphases. Corso Promessi Sposi, 29 Lecco (Italy), Fax: +39 0341499214, tuissi@ieni.cnr.it

ABSTRACT. *Low cycle fatigue of a commercial pseudoelastic Ni-rich Nickel-Titanium alloy has been analysed in this investigation. Fatigue tests have been carried out within the stress-induced transformation regime, by using flat dog-bone shaped specimens obtained from as-received NiTi sheets. In particular, the tests have been executed in two subsequent steps: i) material stabilization and ii) fatigue life estimation. In the first step a variable strain ratio was adopted, in order to avoid compression stresses during unloading, and the strain ratcheting mechanisms have been recorded, up to a stable mechanical response of the alloy. Subsequently, the stabilized specimens have been subjected to strain controlled fatigue tests, under a fixed strain ratio, up to complete failure. Results on functional fatigue, i.e. in terms of stabilized pseudoelastic response, and on structural fatigue, in terms of cycles to failure, are reported and discussed. Furthermore, experimental data have been analysed within the framework of a recent phenomenological strain-life model, based on a modified Coffin-Manson approach. Finally, the fracture surfaces have been analysed by scanning electron microscopy (SEM) in order to analyse the stable and unstable crack growth mechanisms.*

INTRODUCTION

The use of Nickel-Titanium based shape memory alloys (SMAs) is continuously increasing in many branches of engineering and medicine due to their good functional properties, mechanical performance and biocompatibility [1]. However, NiTi alloys exhibit unusual fracture and fatigue responses, if compared with common engineering metals, due to their stress-induced and/or thermally-induced microstructural evolutions. As a consequence, well known theoretical models and standard testing procedures, to analyze the nucleation and propagation of cracks under fatigue loads, cannot be applied to SMAs. To this aim, starting from the pioneer work by Melton and Mercier [2], some experimental studies have been carried out in the last few years to analyze the fatigue behavior of NiTi alloys, by using non-standard specimens and testing procedures [3, 4]. In particular, in most of these works the cyclic behavior of NiTi wires [5-14] and tubes [15-22] have been analyzed, in terms of both crack propagation and fatigue life. These latter studies provide very interesting results since NiTi tubes are employed for the manufacturing of endovascular stents. Moreover, in order to better investigate the fatigue properties of such components, diamond-shaped samples were studied [23, 24],

with geometry very close to the unit cell of a stent. Furthermore, other studies have been devoted to the analysis of the functional fatigue of single crystal NiTi alloys [25, 26] by using special test specimens, which have been cut along different crystallographic orientations. Unfortunately, despite the significant research interest on this topic in the last years, a direct transfereability of the fatigue results to the engineering community is not possible, as fatigue properties of NiTi alloys are significantly affected by the stress and/or thermally induced phase transition mechanisms. As a consequence, well known theories for fatigue life estimation of common metallic alloys cannot be directly applied. In this context, the present study is focused on the low cycle fatigue of a pseudoelastic NiTi sheet in the stress-induced transformation regime, *i.e.* with maximum deformations within the transformation plateau of the alloy. The tests have been carried out in two subsequent steps: i) material stabilization and ii) fatigue life estimation. In the first step a variable strain ratio was adopted, in order to avoid compression stresses during unloading, and the strain ratcheting mechanisms have been recorded, up to a stable mechanical response of the alloy. Subsequently, the stabilized specimens have been subjected to strain controlled fatigue tests, under a fixed strain ratio, up to complete failure. Results on functional fatigue, *i.e.* in terms of stabilized pseudoelastic response, and on structural fatigue, in terms of cycles to failure, are reported and discussed. Furthermore, experimental data have analysed within the framework of a recent phenomenological strain-life model [27], based on a modified Coffin-Manson approach. Finally, the fracture surfaces have been analysed by scanning electron microscopy (SEM) in order to evaluate the stable and unstable crack growth mechanisms.

MATERIAL AND EXPERIMENTAL METHODS

A commercial pseudoelastic Ni-rich NiTi sheet (50.8at.% Ni - 49.2 at.% Ti, Memry, Germany) with thickness $t=1.5$ mm, has been analyzed. Dog bone shaped specimens, with rectangular cross section (1.5mm x 3.5 mm) and with a gauge length of 10 mm, have been made from as received sheets, by wire electro discharge machining. A successive polishing procedure of the machined surfaces was carried out, by sandpapers with progressively finer grits (#400-#1200) and diamond compound (5 μ m). Fatigue test have been carried out, under isothermal condition ($T=298$ K) by using a universal testing machine (Instron 8500) equipped with a climatic chamber (MTS 651). Figure 1 shows a schematic depiction of the stress-strain behavior of a pseudoelastic NiTi alloy together with the values of the measured mechanical parameters, in terms of Young's moduli (E_A , E_M), transformation stresses (σ_s^{AM} , σ_f^{AM} , σ_s^{MA} , σ_f^{MA}) and transformation strain (ε_L). Furthermore, the figure schematically shows the elastic and inelastic strain range ($\Delta\varepsilon_e$, $\Delta\varepsilon_i$) corresponding to the applied total strain range ($\Delta\varepsilon$) in the strain controlled fatigue tests. However, due to the cyclic creep-like behavior of NiTi alloys, which causes the accumulation of residual deformations in the first mechanical cycles ($\delta\varepsilon_{resi}$), as illustrated in Fig. 2, fatigue tests have been carried out in two subsequent steps: 1) Material stabilization and 2) Fatigue life estimation. In particular, in the first step a variable strain ratio was adopted, in order to avoid compression stresses during

unloading, and the strain ratcheting mechanisms have been analyzed up to a stable mechanical response of the alloy corresponding to N_s cycles, namely the number of cycles to material stabilization.

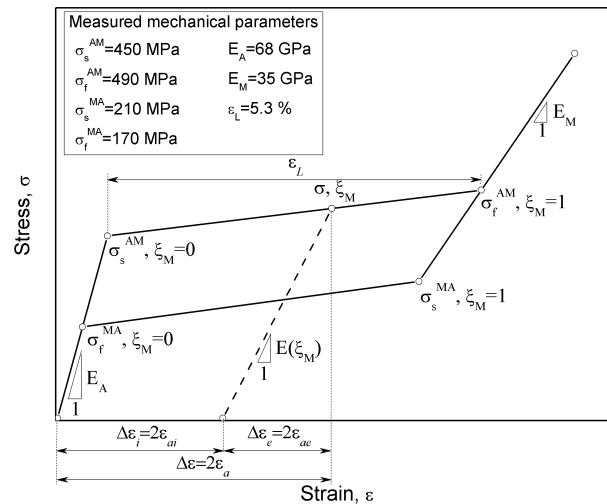


Figure 1. Schematic depiction of the stress strain behavior of the pseudo elastic NiTi alloy together with the main measured mechanical parameters.

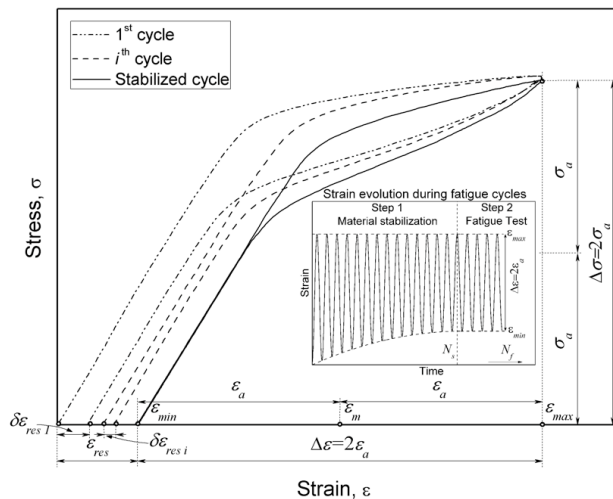


Figure 2. Schematic depiction of the evolution of the stress-strain hysteresis loop under cyclic loadings at fixed values of maximum strain.

The tests have been carried out with maximum strain (ϵ_{max}) within the stress-strain transformation plateau, *i.e.* in the range 0.7-4.5%, and the stabilized values of the residual strain and the recovery strain, ϵ_{res} and ϵ_{rec} respectively, have been recorded (see Fig. 2). In the second step, the specimens have been subjected to strain controlled fatigue cycles at a frequency of 0.5 Hz, under a fixed strain ratio and with a strain range $\Delta\epsilon = 2 \epsilon_a$, up to complete failure and the corresponding number of cycles N_f has been recorded.

RESULTS AND DISCUSSION

Functional fatigue

The cyclic creep-like mechanisms occurring during the first N_s mechanical cycles, mainly due to the formation and accumulation of residual martensite, can be considered as a functional fatigue damage phenomenon, as it causes a decrease of the pseudoelastic recovery capability of the alloy. An accurate knowledge of this functional degradation is essential for the design of NiTi based components as they are normally subjected to repeated thermo-mechanical cycles. Figure 3 illustrates the stabilized recovery and residual deformations (ε_{rec} and ε_{res}) as a function of the maximum applied strain (ε_{max}), in a log-log diagram.

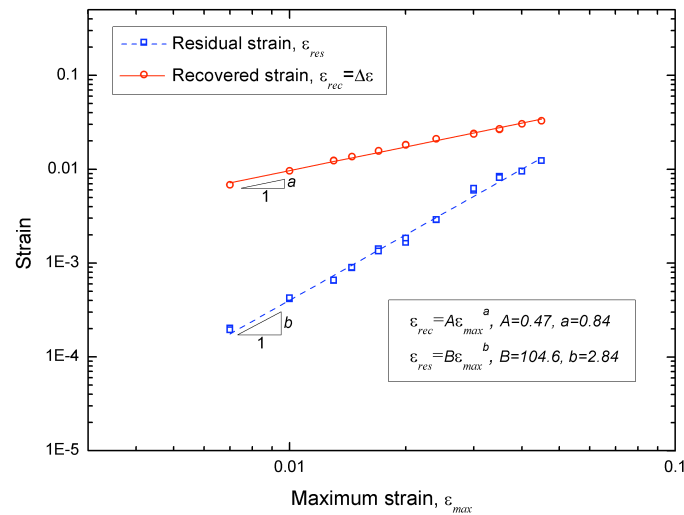


Figure 3. Stabilized residual strain and recovered strain (ε_{rec} and ε_{res}) as a function of the applied maximum strain (ε_{max}).

As expected the figure shows that ε_{res} increases with increasing the maximum strain, from about 0.02% at $\varepsilon_{max} = 0.7\%$ to 1.24% at $\varepsilon_{max} = 4.5\%$, and, consequently, the recovery strain, ε_{rec} , ranges between 0.68% and 3.26% ($\varepsilon_{rec} = \varepsilon_{max} - \varepsilon_{res}$). Furthermore, the figure shows that experimental data are well approximated by straight lines in the log-log diagram and, consequently, ε_{rec} and ε_{res} can be expressed by:

$$\varepsilon_{res} = A\varepsilon_{max}^a \quad (1)$$

$$\varepsilon_{rec} = B\varepsilon_{max}^b \quad (2)$$

where the coefficients A and B and the exponents a and b are given in Fig. 3. In addition, the number of cycles to material stabilization, N_s , is mainly unaffected by the maximum applied strain and it is in range between 100 and 150.

Structural fatigue

Fatigue data have been analyzed within the framework of a recent literature approach [27] which is based on a modified Coffin-Manson relationship [28]. In particular, as

illustrated in Fig. 1, the total strain range, $\Delta\varepsilon$, can be decomposed in the elastic strain, $\Delta\varepsilon_e$, and inelastic strain, $\Delta\varepsilon_i$, which can be regarded as the pseudoelastic recovery:

$$\Delta\varepsilon = \Delta\varepsilon_e + \Delta\varepsilon_i \quad (3)$$

where the elastic strain is calculated based on the assumption of linear evolution of the martensite fraction, ξ_M , along the stress-strain transformation plateau [29] and on the use of the Reuss's formula [30] to estimate the Young's modulus, $E(\xi_M)$, (see Fig. 1):

$$\Delta\varepsilon_e = \Delta\sigma/E(\xi_M) \quad (4)$$

In addition, eq. 3 can be expressed as a function of the strain amplitudes ($\varepsilon_a = \Delta\varepsilon/2$):

$$\varepsilon_a = \varepsilon_{ae} + \varepsilon_{ai} \quad (5)$$

Figure 4 illustrates the elastic, inelastic and total strain amplitude (ε_{ae} , ε_{ai} and ε_a) as a function of the number of cycle reversals to failure ($2N_f$) in a log-log diagram.

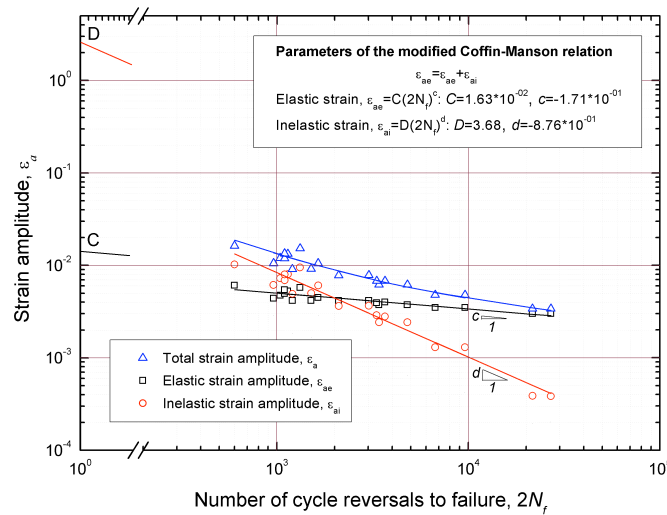


Figure 4. Modified Coffin-Manson approach.

Furthermore, the figure shows that both elastic and inelastic strain amplitude (ε_{ae} and ε_{ai}) are well approximated by straight lines in the log-log diagram and, consequently, the two strain components can be expressed by a power law relations in the $\varepsilon_a - 2N_f$ diagram, likewise to Coffin-Manson approach in common engineering metals.

In particular, the total strain amplitude, ε_a , can be related to the cycle reversals to failure, $2N_f$, based on a modified Coffin-Manson approach:

$$\varepsilon_a = \varepsilon_{ae} + \varepsilon_{ei} = C (2N_f)^c + D (2N_f)^d \quad (6)$$

where the coefficients C and D and the exponents c and d obtained from the experiments are reported in Fig. 4. It is worth noting that these values have been

obtained from a fitting of the experimental data reported in this investigation, *i.e.* they are related to specific specimen geometry and loading conditions and, consequently, they should be considered as testing parameters. However, the transferability of the proposed model to the engineering community, *i.e.* to predict fatigue life under generic loading conditions, requires further systematic experimental tests. Furthermore, the results presented in this paper have been obtained with maximum deformation within the stress-induced transformation regime and, consequently, the fatigue response of the material in the full austenitic and martensitic regions has not been investigated.

SEM analyses of the fracture surfaces

In Fig. 5 are depicted the SEM micrographs of the fracture surfaces obtained by testing the samples at different values of maximum deformation (a. 0,7%, b. 1,3%, c. 1,45%, d. 1,7%). The analysis revealed that crack initiation occurs at the lateral surface of the specimens, as a consequence of the surface defects produced by the cutting process. In fact, these irregularities lead to local stress concentrations and act as preferable nucleation sites. Furthermore, fracture surfaces show two distinct regions characterized by different morphologies. In particular, the right part of the surfaces in the SEM micrographs of Fig. 5 are characterized by fatigue striations, which are attributed to the stable crack growth resulting from fatigue loads, while the left sides show dimples structures typical of ductile overload fractures. In addition, as expected, the stable crack penetration area decreases with increasing of the maximum applied deformation, ranging from about 2.8 mm at $\varepsilon_{max} = 0.7\%$ to 0.8 mm at $\varepsilon_{max} = 1.7\%$.

CONCLUSION

Strain controlled fatigue tests of a commercial pseudoelastic NiTi alloy, have been carried out within the stress-induced transformation regime. Both functional and structural fatigue have been analyzed, *i.e.* the evolution of the pseudoelastic capability and the cycles to failure. The results revealed a degradation of the pseudoelastic recovery, during the first mechanical cycles, and this effect becomes more evident when increasing the strain amplitude. However, a stable functional response is always observed after the first stabilization cycles, which occurs between 100 and 150 cycles. Furthermore, structural fatigue data have been analyzed by a novel strain-life model, based on a modified Coffin-Manson approach. Finally, fracture surfaces have been analyzed by SEM observation in order to study the stable and unstable crack growth mechanisms. However, future experimental tests should be carried out to validate the model and, consequently, to allow a direct transferability of the fatigue data to the engineering community.

ACKNOWLEDGMENT

The authors wish to thank Giordano Carcano (CNR IENi Lecco) for SEM technical assistance.

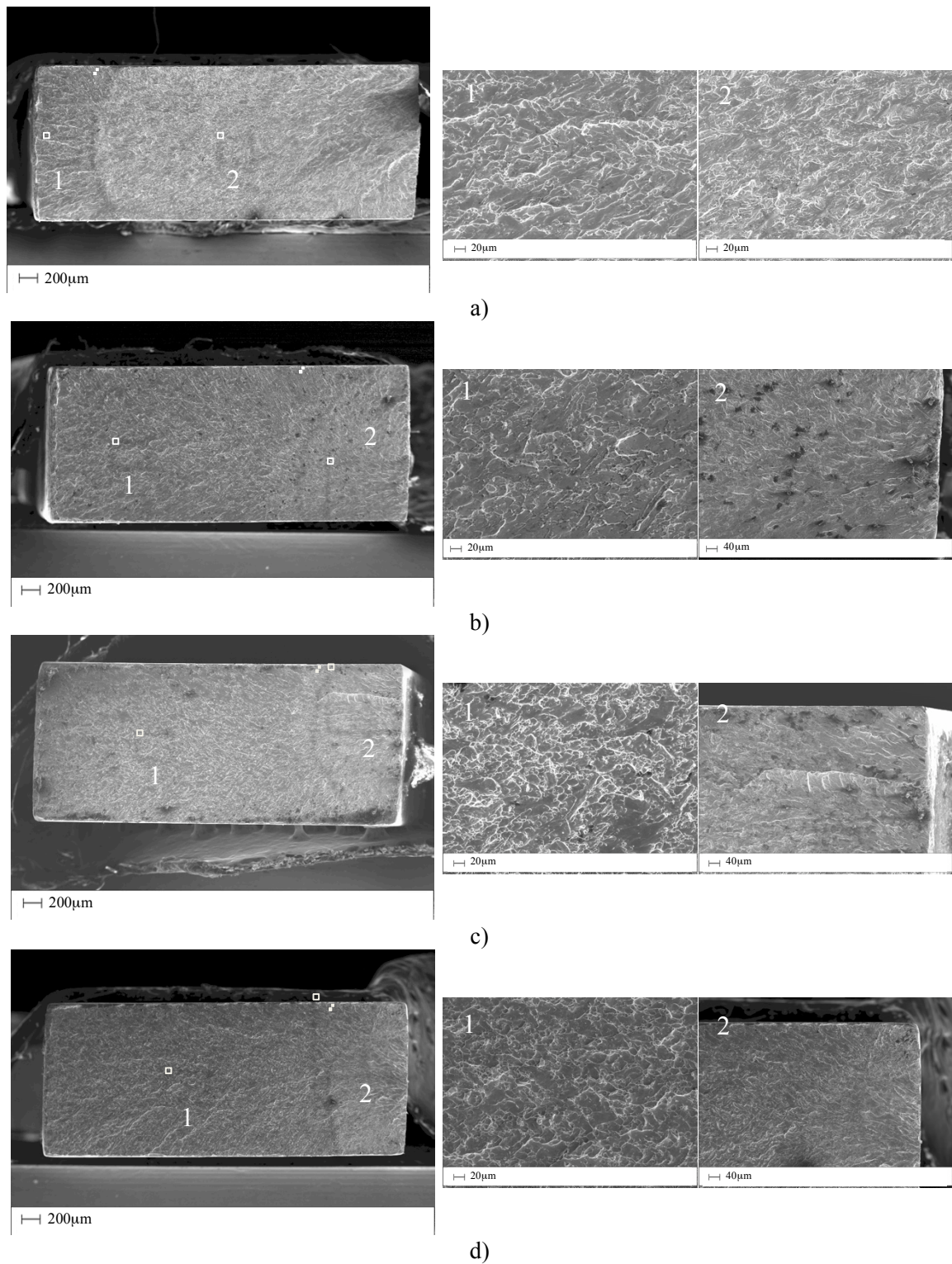


Figure 5. SEM micrographs of the fracture surfaces with highlight of the stable (right) and unstable (left) crack growth path obtained from specimens tested at different values of maximum deformation: a) 0.7%, b) 1.3%, c) 1.45% and d) 1.7%.

REFERENCES

1. Otsuka, K., Ren, X. (2005) *Progr. Mater. Sci.* **50**, 511-678
2. Melton, K.N., Mercier, O. (1979) *Acta Metall.* **27**, 137-144
3. Hornbogen, E. (2004) *J. Mater. Sci.* **39**, 385-399
4. Pelton, A.R. (2011) *J. Mater. Eng. Perform.* **20**, 613-617
5. Miyazaki, S., Imai, T., Igo, Y., Otsuka, K. (1986) *Metall. Trans A.* **17**, 115-120
6. Tobushi, H., Shimeno, Y., Hachisuka, T., Tanaka, K. (1998) *Mech. Mater.* **30**, 141-150
7. Lagoudas, D.C., Miller, D.A., Rong, L., Kumar, P.K. (2009) *Smart Mater. Struct.* **18** art no. 085021
8. Soul, H., Isalgue, A., Yamny, A., Torra, V., Lovey, F.C. (2010) *Smart Mater. Struct.* **19**, 1-7
9. Dolce, M., Cardone, D. (2001) *Int. J. Mech. Sci.* **43**, 2657-2677
10. Miyazaki, S., Mizukoshi, K., Ueki, T., Sakuma, T., Liu, Y. (1999) *Mater. Sci. Eng.* **A273-275**, 658-663
11. Tobushi, H., Nakahara, T., Shimeno, Y., Hashimoto, T. (2000) *J. Eng. Mater-T ASME.* **122**, 186-191
12. Eggeler, G., Hornbogen, E., Yawny, A., Heckmann, A., Wagner, M. (2004) *Mater. Sci. Eng. A* **378**, 24-33
13. Figueiredo, A.M., Modenesi, P., Buono, V. (2009). *J. Fatigue.* **31**, 751-758
14. Norwich, D.W., Fasching, A. (2009) *J. Mater. Eng. Perform.* **18**, 558-562
15. Nemat-Nasser, S., Guo, W.G. (2006) *Mech. Mater.* **38**, 463-474
16. Kang, G., Kan, Q., Yu, C., Song, D., Liu, Y. (2012) *Mater. Sci. Eng. A* **535**, 228- 234
17. Casciati, S., Marzi, A. (2011) *Eng. Struct.* **33**, 1232-1239
18. McKelvey, A.L., Ritchie, R.O. (1999) *J. Biomed. Mater. Res.* **47**, 301-308
19. McKelvey, A.L., Ritchie, R.O. (2001) *Metall. Mater. Trans. A.* **32A**, 731-743
20. Tabalni, R.M., Simha, N.K., Berg, B.T. (2001) *Metall. Mater. Trans. A.* **32A**, 1866-1869
21. Runciman, A., Xu, D., Pelton, A.R., Ritchie, R.O. (2011) *Biomaterials.* **32**, 4987-4993
22. Moumni, Z., Van Herpen, A., Riberty, P. (2005) *Smart Mater. Struct.* **14**, 287-292
23. Pelton, A.R., Gong, X.Y., Duerig, T. (2003) *Medical Device Materials – Proceedings of the Materials and the Processes for Medical Devices Conference 2003*, 199-204
24. Pelton, A.R., Schroeder, V., Mitchell, M.R., Gong, X.Y., Barney, M., Robertson, S.W. (2008) *J. Mech Behav Biomed.* **1**, 153-164
25. Gall, K., Sehitoglu, H., Chumlyakov, Y.I., Kireeva, I.V. (1999) *Scripta Mater.* **40(1)**, 7-12
26. Sehitoglu, H., Anderson, R., Karaman, I., Gall, K., Chumlyakov, Y. (2001) *Mater. Sci. Eng. A* **314**, 67-74.
27. Maletta, C., Furgiuele, F., Sgambitterra, E. (2012), Fatigue of pseudoelastic NiTi within the stress-induced transformation regime: a novel strain-life approach, *Submitted in Smart Mater. Struct.*
28. Stephens, R.I., Fatemi, A., Stephens, R.R., Fuchs, H.O. (2000). In: *Metal Fatigue in Engineering*, (second ed.), Wiley-Interscience, New York
29. Maletta, C., Falvo, A., Furgiuele, F., Reddy, J.N. (2009) *Smart Mater. Struct.* **18**, 1-9
30. Auricchio, F., Sacco, E. (1997) *Int. J. NonLin. Mech.* **32**, 1101-1114